Supplementary Information

Strain-Induced Room-Temperature Ferroelectricity in $SrTiO_3$ Membranes

Xu et al.

Supplementary Figure 1

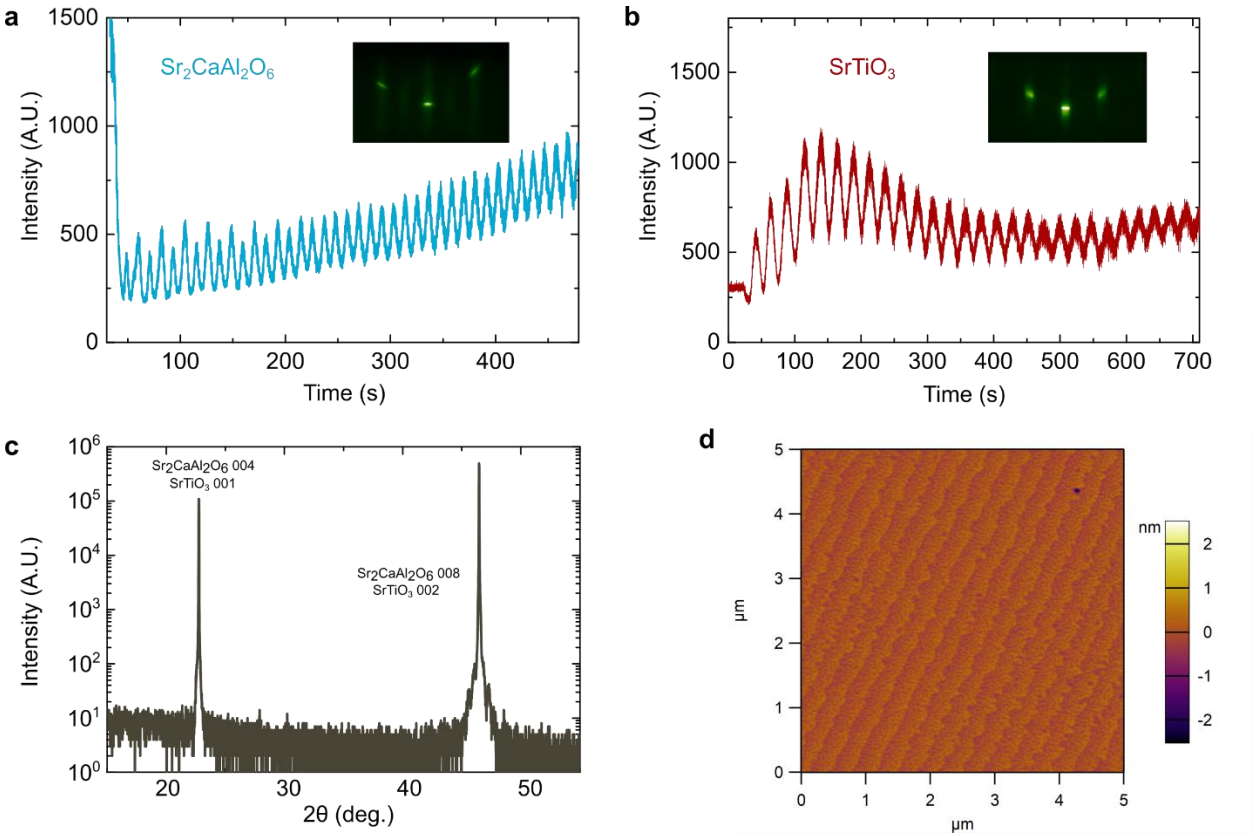

Supplementary Figure 1 | Growth and structural characterization of $SrTiO_3$ / $Sr_2CalAl_2O_6$ / $SrTiO_3$ heterostructure. Reflection high-energy electron diffraction (RHEED) oscillations and patterns of **a**, $Sr_2CaAl_2O_6$ and **b**, $SrTiO_3$, which indicate typical layer-by-layer 2D growth mode. **c**, θ - 2θ X-ray diffraction scans showing a single diffraction peak with all layer peaks overlapping together due to the small lattice mismatch between the different film layers. **d**, Atomic force microscopy characterization of as-grown $SrTiO_3$ films showing an atomically smooth surface with unit cell step terraces.

Supplementary Figure 2

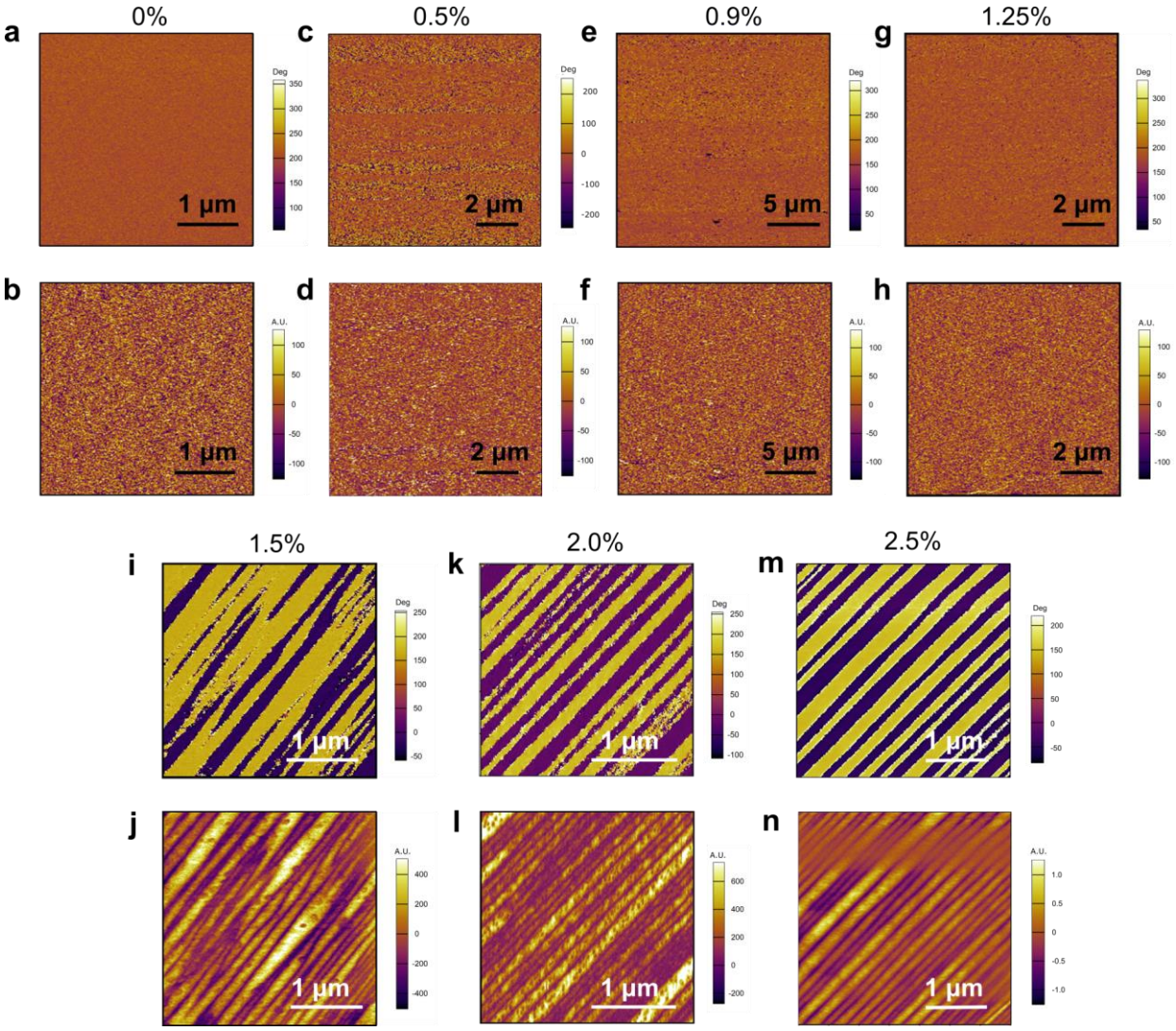

Supplementary Figure 2 | Room-temperature piezoresponse force microscopy (PFM) characterization of strained $SrTiO_3$ membranes. Lateral PFM phase and amplitude of membranes uniaxially strained at **a**, **b**, 0%; **c**, **d**, 0.5%; **e**, **f**, 0.9%; **g**, **h**, 1.25%; **i**, **j**, 1.5%; **k**, **l**, 2.0%; **m**, **n**, 2.5%, respectively, wherein room-temperature ferroelectricity is observed to emerge at 1.5% strain, which is characterized by the 180° ferroelectric polydomain patterns.

Supplementary Figure 3

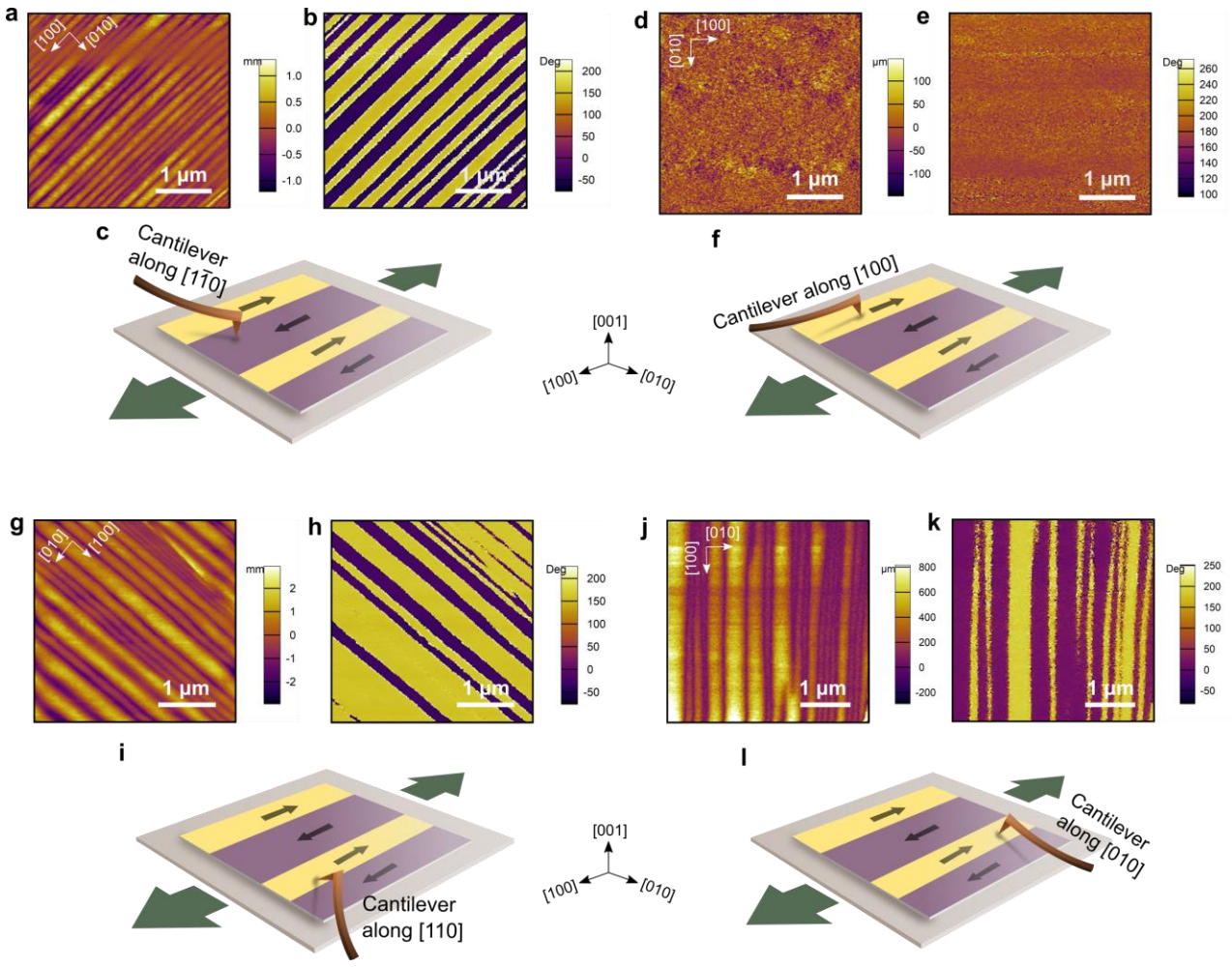

Supplementary Figure 3 | Piezoresponse force microscopy (PFM) characterization of domain structures in 2.5% strained $SrTiO_3$ membranes. Lateral PFM amplitude and phase measured by aligning the PFM cantilever along the **a**, **b**, [1$\bar{1}$0], **d**, **e**, [100], **g**, **h**, [110], and **j**, **k**, [010] directions, respectively. Whereas evident ferroelectric stripe domain patterns are observed when scanning along the [1$\bar{1}$0], [110], and [010] directions, the piezoresponse vanishes when scanning along [100], indicating the in-plane polarization of the ferroelectric domains is aligned along [100]/[$\bar{1}$00], with the adjacent domains polarized at a 180° difference. The measurement process is illustrated in **c**, **f**, **i**, and **l**. These results clearly show that the polarization of these domain features

align along specific crystallographic directions, which evidences the presence of ferroelectricity, whereas other mechanisms of induced ferroelectric-like PFM response are typically invariant with respect to the cantilever scan orientation.

Supplementary Figure 4

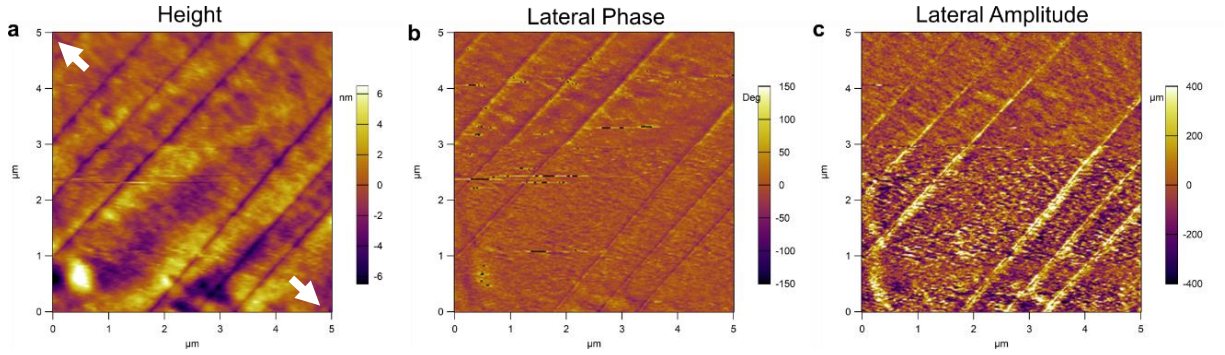

Supplementary Figure 4 | Piezoresponse Force Microscopy (PFM) characterization of strained $SrTiO_3$ membranes beyond the threshold for crack formation. **a**, PFM height image shows cracks perpendicular to the uniaxial strain direction. White arrows illustrate the uniaxial strain direction along [100]. **b**, Lateral phase and **c**, amplitude images show the absence of 180º degree domains in cracked $SrTiO_3$ membranes.

Supplementary Figure 5

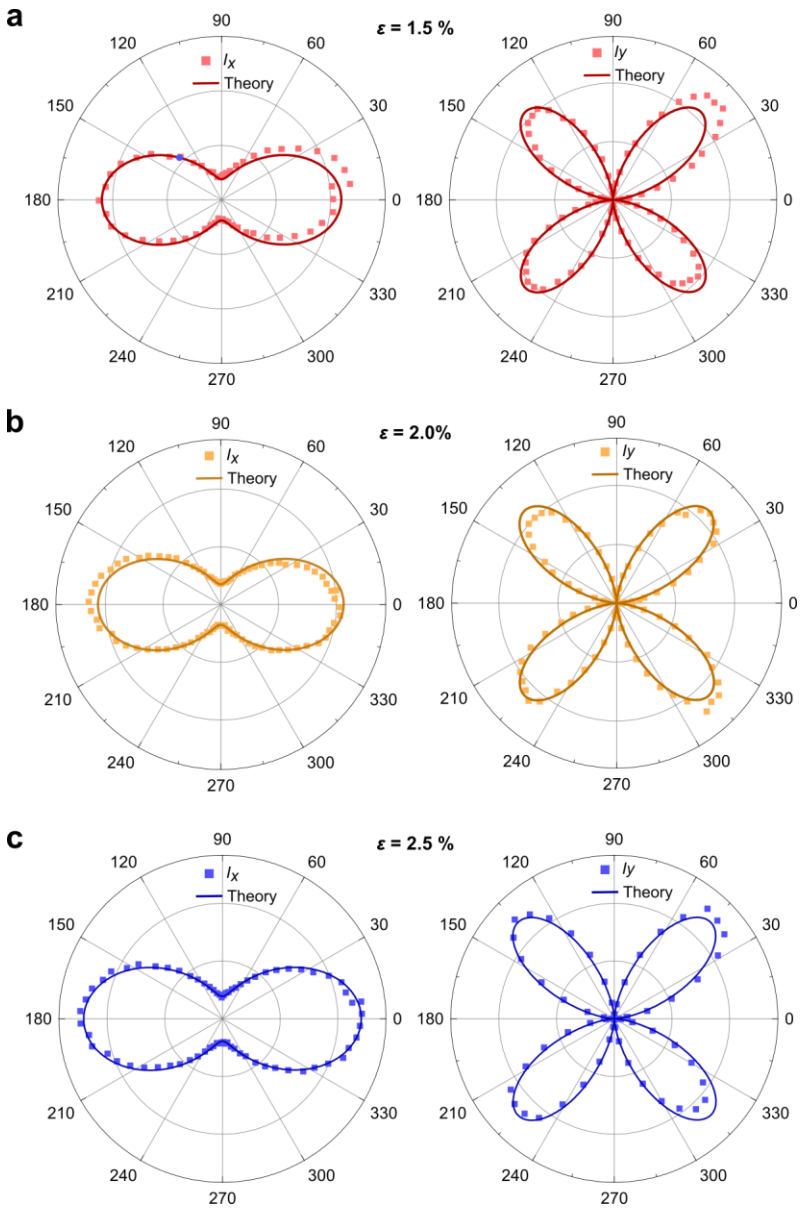

Supplementary Figure 5 | Optical second harmonic generation (SHG) measurements of $SrTiO_3$ membranes. SHG polar plots measured at room temperature as a function of incident beam polarization in membranes strained at **a**, 1.5%, **b**, 2.0%, **c**, 2.5%.

Supplementary Figure 6

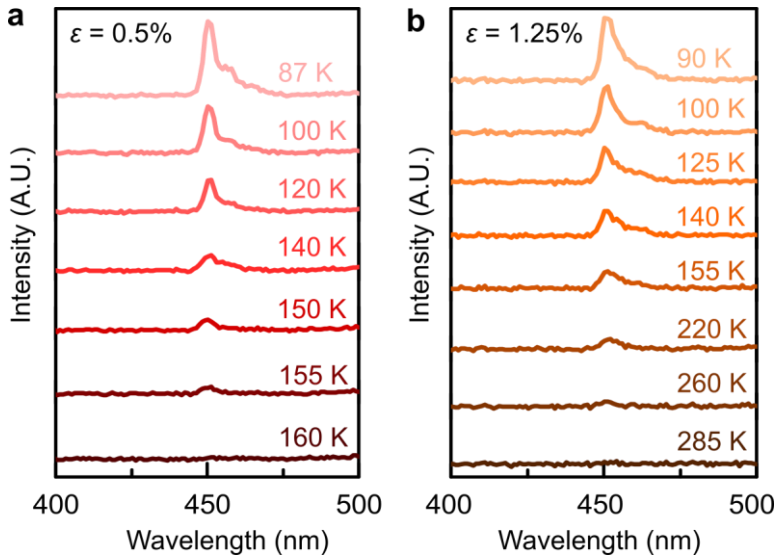

Supplementary Figure 6 | Temperature-dependent second harmonic generation (SHG) measurements of strained $SrTiO_3$ membranes. SHG measurements performed on $SrTiO_3$ membranes as a function of temperature. The membranes are uniaxially strained at **a**, 0.5% and **b**, 1.25%.

Supplementary Figure 7

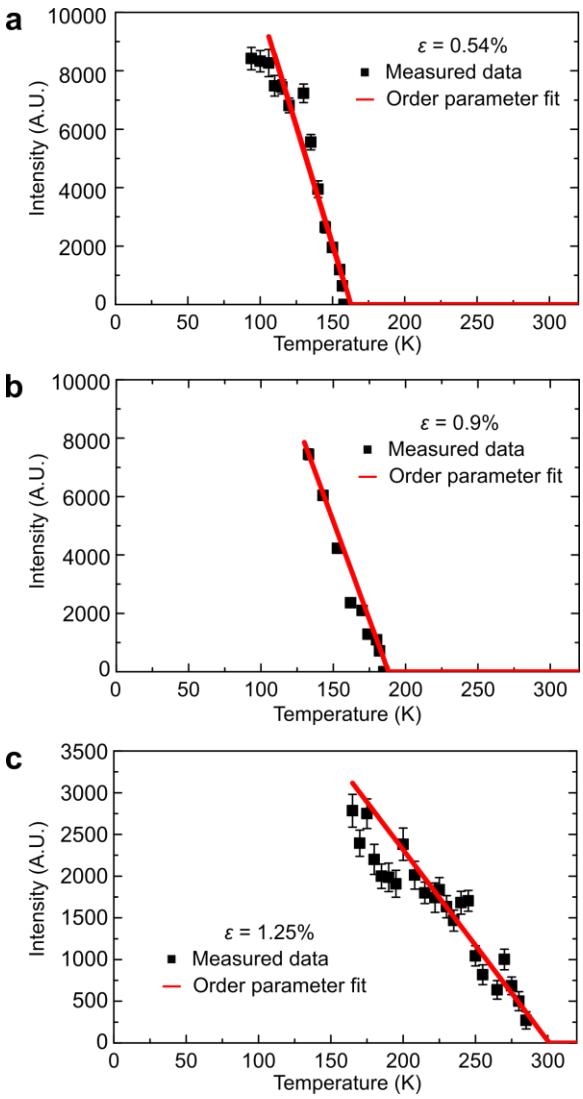

Supplementary Figure 7 | Extracting T_c from SHG results for each strain state. Here, since the SHG intensity $\propto P_1^2$ while $P_1 \propto T^{1/2}$ (within the Ginsburg-Landau-Devonshire model), we can derive that the SHG intensity $\propto T$. Plotting the integrated SHG peak intensity as a function of temperature for membranes uniaxially strained at **a**, 0.54%, **b**, 0.9%, and **c**, 1.25%, the T_c can be extracted for each strain state with this linear intensity-temperature relationship. Error bars represent the standard deviation.

Supplementary Figure 8

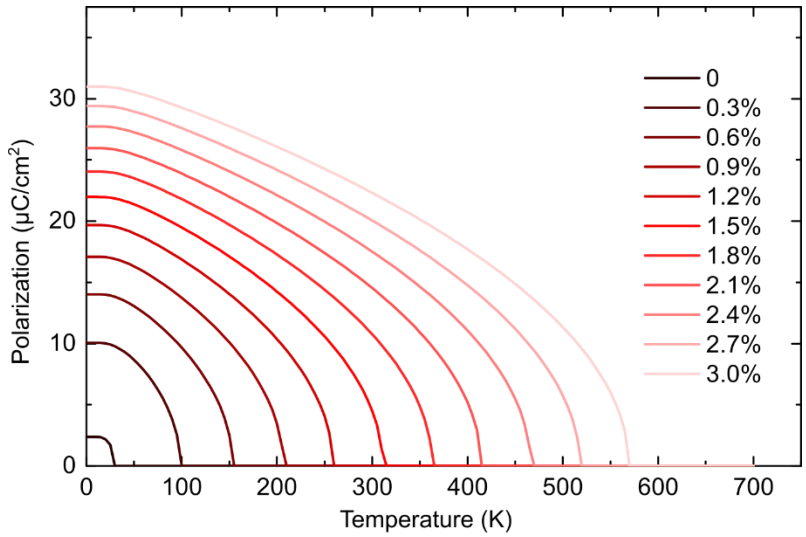

Supplementary Figure 8 | The calculated polarization evolution with temperature at different uniaxial strain states. Temperature-dependent polarization evolution as a function of applied uniaxial strain along [100] is calculated using the Ginsburg-Landau-Devonshire model. The relation between the transition temperature T_c and strain can be further extracted at $P = 0$.

Supplementary Figure 9

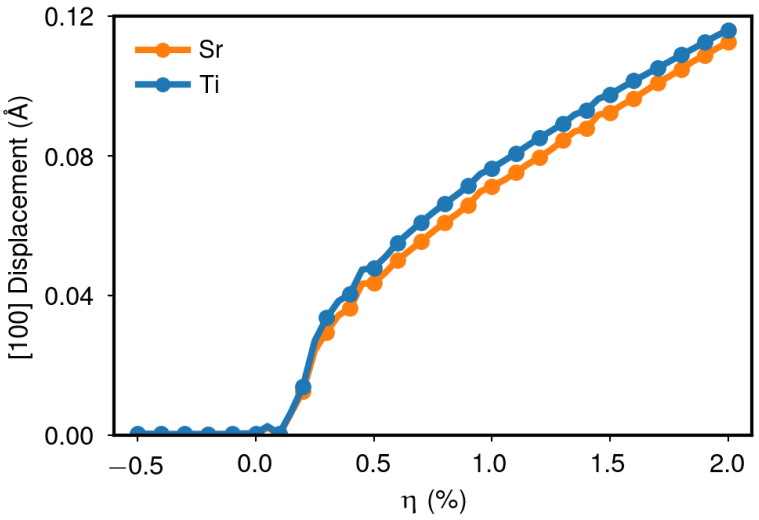

Supplementary Figure 9 | The local displacements of Sr and Ti atoms calculated by DFT. Both the Sr and Ti atoms in $SrTiO_3$ displace along the [100] direction in response to the uniaxial strain along [100].

Supplementary Figure 10

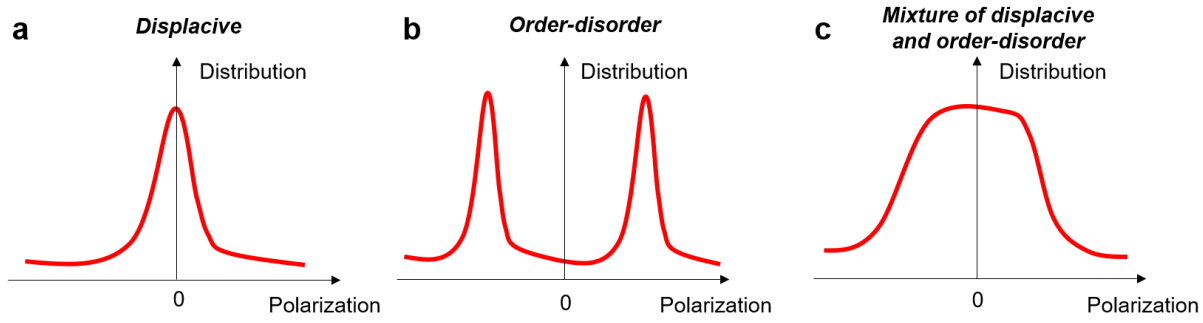

Supplementary Figure 10 | Schematics of the characteristic polarization distribution near the phase transition. The polarization distribution in the paraelectric phase for **a**, displacive, **b**, order-disorder, and **c**, a mixture of the two. In the ferroelectric phase of strained $SrTiO_3$, the displacive character dominates at lower temperature, as the distribution of local polarization has a single peak and the peak position shifts toward lower polarization values with increasing temperature. When the temperature rises close to T_c, the order-disorder character dominates, shown as a double-peak in the distribution curve. However, an ideal order-disorder character will have the two peaks well separated in the high temperature phase. Therefore, even at a temperature close to T_c, the displacive character still plays a role, indicating a mixture of displacive and order-disorder transition characteristics in $SrTiO_3$.

Supplementary Table 1. DFT calculated structural evolution with uniaxial strain

Strain (%)	*a* (Å)	*b* (Å)	*c* (Å)	P_x (C m^{-2})	P_y (C m^{-2})	P_z (C m^{-2})
-0.5	3.8377	3.857	3.8617	0.001	0	0
-0.45	3.8396	3.857	3.8617	0.001	0	0
-0.4	3.8416	3.857	3.8606	0.001	0	0
-0.35	3.8435	3.857	3.86	0.001	0	0
-0.3	3.8454	3.857	3.8595	0.001	0	0
-0.25	3.8474	3.857	3.859	0.001	0	0
-0.2	3.8493	3.857	3.8586	0.001	0	0
-0.15	3.8512	3.857	3.8578	0.001	0	0
-0.1	3.8531	3.857	3.8573	0.001	0	0
-0.05	3.8551	3.857	3.8548	0.001	0	0
0	3.857	3.857	3.8548	0.001	0	0
0.05	3.8589	3.857	3.8554	-0.007	0	0
0.1	3.8609	3.857	3.855	0.001	0	0
0.15	3.8628	3.857	3.8543	0.018	0	0
0.2	3.8647	3.857	3.8539	0.037	0	0
0.25	3.8666	3.857	3.8534	0.072	0.001	0
0.3	3.8686	3.857	3.8529	0.09	0.001	0
0.35	3.8705	3.857	3.8525	0.103	0.001	0
0.4	3.8724	3.857	3.8516	0.109	0.001	0
0.45	3.8744	3.857	3.8515	0.128	0.001	0
0.5	3.8763	3.857	3.8508	0.129	0.001	0
0.55	3.8782	3.857	3.8501	0.137	0.002	0
0.6	3.8801	3.857	3.8496	0.148	0.002	0
0.65	3.8821	3.857	3.8493	0.156	0.002	0
0.7	3.884	3.857	3.8488	0.164	0.002	0
0.75	3.8859	3.857	3.8482	0.171	0.002	0
0.8	3.8878	3.857	3.8472	0.178	0.002	0
0.85	3.8898	3.857	3.8466	0.185	0.002	0
0.9	3.8917	3.857	3.8466	0.192	0.003	0
0.95	3.8936	3.857	3.8455	0.202	0.003	0
1	3.8956	3.857	3.8454	0.206	0.003	0
1.05	3.8975	3.857	3.8448	0.211	-0.007	0.001
1.1	3.8994	3.857	3.8443	0.217	-0.007	0.001
1.15	3.9013	3.857	3.8417	0.224	-0.007	0.001
1.2	3.9033	3.857	3.8425	0.229	-0.007	0.001
1.25	3.9052	3.857	3.8405	0.235	-0.007	0.001
1.3	3.9071	3.857	3.8412	0.241	-0.007	0.001
1.35	3.9091	3.857	3.8405	0.248	-0.008	0.001
1.4	3.911	3.857	3.8385	0.251	-0.006	0.001
1.45	3.9129	3.857	3.84	0.26	-0.011	0.002
1.5	3.9148	3.857	3.8395	0.263	-0.013	0.003
1.55	3.9168	3.857	3.8383	0.269	-0.011	0.003

1.6	3.9187	3.857	3.8384	0.274	-0.012	0.004
1.65	3.9206	3.857	3.8376	0.279	-0.012	0.004
1.7	3.9226	3.857	3.8371	0.284	-0.014	0.001
1.75	3.9245	3.857	3.8366	0.289	-0.014	0.002
1.8	3.9264	3.857	3.8354	0.294	-0.013	0.002
1.85	3.9284	3.857	3.8356	0.299	-0.016	-0.001
1.9	3.9303	3.857	3.8349	0.304	-0.013	0.003
1.95	3.9322	3.857	3.8342	0.309	-0.012	0.003
2	3.9341	3.857	3.8336	0.314	-0.009	0.003

Supplementary Table 2. Landau Free Energy Parameters for $SrTiO_3$

Parameters	Value (in cgs units, temperature in K)
α_1	$4.5[\coth\left(\frac{54}{T}\right) - \coth\left(\frac{54}{30}\right)] \times 10^{-3}$
α_{11}	2.5×10^{-12}
α_{12}	1.5×10^{-12}
c_{11}	3.36×10^{12}
c_{12}	1.07×10^{12}
c_{44}	1.27×10^{12}
g_{11}	1.39
g_{12}	-0.12
g_{44}	0.27
β_{11}	1.94×10^{43}
β_{12}	3.96×10^{43}
λ_{11}	1.3×10^{27}
λ_{12}	$- 2.5 \times 10^{27}$
λ_{44}	$- 2.3 \times 10^{27}$
t_{11}	$- 3.74 \times 10^{15}$
t_{12}	0.15×10^{15}
t_{44}	7.0×10^{15}